

Electrostatically induced superconductivity at the surface of WS_2

Sanghyun Jo,[†] Davide Costanzo,[†] Helmut Berger,[‡] and Alberto F. Morpurgo^{*,†}

DQMP and GAP, Université de Genève, 24 quai Ernest Ansermet, CH-1211 Geneva, Switzerland, and Institut de Physique de la Matière Complexe, Ecole Polytechnique Fédérale de Lausanne, CH-1015 Lausanne, Switzerland

E-mail: Alberto.Morpurgo@unige.ch

KEYWORDS: WS_2 , Transition metal dichalcogenides, Ionic liquid gating, Superconductivity, Potential fluctuation, BKT transition

Abstract

We investigate transport through ionic liquid gated field effect transistors (FETs) based on exfoliated crystals of semiconducting WS_2 . Upon electron accumulation, at surface densities close to –or just larger than– 10^{14} cm^{-2} , transport exhibits metallic behavior, with the surface resistivity decreasing pronouncedly upon cooling. A detailed characterization as a function of temperature and magnetic field clearly shows the occurrence of a gate-induced superconducting transition below a critical temperature $T_c \approx 4 \text{ K}$, a finding that represents the first demonstration of superconductivity in tungsten-based semiconducting transition metal dichalcogenides. We investigate the nature of superconductivity and find significant inhomogeneity, originating from the local detaching of the frozen ionic liquid from the WS_2 sur-

*To whom correspondence should be addressed

[†]DQMP and GAP, Université de Genève, 24 quai Ernest Ansermet, CH-1211 Geneva, Switzerland

[‡]Institut de Physique de la Matière Complexe, Ecole Polytechnique Fédérale de Lausanne, CH-1015 Lausanne, Switzerland

face. Despite the inhomogeneity, we find that in all cases where a fully developed zero resistance state is observed, different properties of the devices exhibit a behavior characteristic of a Berezinskii-Kosterlitz-Thouless transition, as it could be expected in view of the two-dimensional nature of the electrostatically accumulated electron system.

Semiconducting transition metal dichalcogenides (TMDs; chemical formula MX_2 , with $\text{M} = \text{Mo}, \text{W}$ and $\text{X} = \text{S}, \text{Se}, \text{Te}$) have been recently attracting considerable interest. Being van der Waals layered materials, thin crystalline flakes can be extracted out of bulk crystals by mechanical exfoliation, and allow the realization of high-quality two-dimensional (2D) electronic systems with unique properties.^{1,2} From a fundamental perspective, for instance, the absence of inversion symmetry,¹⁻³ a strong spin-orbit interaction,¹⁻³ and the direct nature of the band-gap^{4,5} in monolayers give unique control over the valley and the spin degrees of freedom.^{3,6-11} Additionally, high-quality field-effect transistors (FETs)¹²⁻¹⁹ and different kinds of opto-electronic devices^{10,17,20-26} have been demonstrated, which may be in principle advantageous for future applications.

Another reason that has attracted attention to these materials is the occurrence of superconductivity upon accumulation of electrons at the surface of MoS_2 and MoSe_2 , as it has been observed in a FET configuration.²⁷⁻²⁹ Key to this result is the use of ionic liquid for electrostatic gating,^{30,31} which enables density of carriers in excess of $n = 10^{14} \text{ cm}^{-2}$ to be accumulated at the material surface, a much larger value than that accessible in FETs with conventional solid dielectrics. The possibility to induce superconductivity electrostatically is particularly appealing as compared to other methods (e.g., doping by intercalation^{32,33}) because it does not cause structural modifications in the material, and therefore it is likely to affect less its electronic band structure (or at least to affect it in a more controlled way, since the result of intercalation depends strongly on the spatial arrangement of the intercalant atoms). Additionally, the technique allows exploring superconductivity in carrier density ranges that may not be accessible by intercalation, as it has been recently reported for MoS_2 (where a lower carrier density unexpectedly gives rise to a larger critical temperature).²⁷

So far, only a very limited amount of work on electrostatically induced superconductivity in

ionic liquid gated TMDs has been reported,^{27–29} and many different interesting questions remain to be answered. One is whether the possibility to induce superconductivity electrostatically is confined to Mo-based compounds (the only ones in which the phenomenon has been observed so far), or whether it is more general. Indeed, recent low-temperature transport measurements of ionic liquid gated WSe₂ FETs have not revealed the occurrence of a superconducting transition for T as low as 1.5 K, despite the accumulation of surface electron densities significantly larger than $\sim 10^{14} \text{ cm}^{-2}$.³⁴ Other questions concern the nature of superconductivity, specifically the homogeneity of the superconducting state, and whether signatures can be found in the experiments of the 2D character^{35–41} of the superconducting transition, which can be expected given that at $n \sim 10^{14}$ the thickness of the electron accumulation layer at surface⁴² is approximately 1 nm.

We have addressed these issues by performing investigations of low-temperature transport in ionic liquid gated FETs realized on thin exfoliated crystals of WS₂. At sufficiently high gate voltage –corresponding to accumulated surface carrier density of $n \simeq 10^{14}$ – we observe that the square resistance initially decreases upon cooling, and then saturates when T is lowered below 40 K, a clear manifestation of metallic behavior. Upon further cooling, a sharp decrease in resistivity is observed with an onset at approximately 4 K, leading to a zero resistance state at $T \simeq 0.5\text{K}$ (the precise values of temperature depend on the device and on the cool-down). The application of a perpendicular magnetic field B results in the destruction of the zero-resistance state (already at very low B) and in a progressive increase of the device resistance, which at $B \simeq 0.1 \text{ T}$ reaches the normal state value. These observations provide a clear experimental demonstration of the occurrence of electrostatically induced superconductivity at the surface of WS₂.

We further investigate the properties and character of the superconducting state, by performing measurements on devices with many different pair of contacts, which allow us to characterize transport locally. Although, a clear signature of the superconducting transition is generally observed irrespective of the part of the device probed, a strong inhomogeneity in square resistance, carrier density and critical temperature are also regularly observed. We attribute the inhomogeneity to the frozen ionic liquid that locally detaches from the WS₂ surface, resulting in large variation

of the local capacitance, and therefore of the density of accumulated charge. Despite these inhomogeneities, we find that the temperature-dependent $I - V$ curves measured in the regions of the devices where a zero-resistance state is observed exhibit the behavior typically associated to 2D superconductors³⁵⁻⁴¹ of the Berezinskii-Kosterlitz-Thouless (BKT) type. Besides providing the first demonstration of electrostatically induced superconductivity at the surface of WS₂, our findings reveal different interesting aspects of ionic-liquid gated devices that are certainly relevant to understand the low- T normal and superconducting transport properties of these systems.

Fig. 1(a) shows an optical microscope image of a 20 nm thick WS₂ flake. The flake was exfoliated from a bulk crystal and transferred onto a Si/SiO₂ substrate. Contacts consist of a Ti/Au (10/50 nm) bilayer and were defined by conventional nano-fabrication techniques (electron-beam lithography, metal evaporation and lift-off). Together with the contacts, a large-area pad acting as gate was also defined (see Fig. 1(b) for the schematic device configuration). To form the ionic gated FET, a small droplet of ionic liquid DEME-TFSI was placed onto the device (Fig. 1(b)) in the controlled environment of a glove-box, after which the device was rapidly transferred in the vacuum chamber of a 3He cryostat used for the T -dependent transport measurements. Before starting the measurements, the device was left in vacuum, at room temperature, at a pressure of $\approx 10^{-6}$ mbar for one day to remove humidity and oxygen present in the ionic liquid. Three similar devices were investigated in detail, with multiple cool-downs at different values of gate voltage, and exhibited virtually identical transport behavior; here we show data from one of them which is representative of this behavior.

We start with the characterization of the device room-temperature transport properties. The transfer curve (i.e., the source-drain (S-D) current I_{SD} measured as a function of gate voltage V_G) is shown in Fig. 1(c) for a source-drain bias $V_{SD} = 1$ mV. The data exhibit clear ambipolar transport, similarly to what we have reported previously.¹⁴ To eliminate contact effects and to check the device homogeneity, we measured four-terminal resistances using as voltage probes different, adjacent pairs of contacts (numbered from 1 to 10 in Fig. 1(a); in all cases –here and in the remainder of this paper, if not stated otherwise– the current is sent from the S to the D contact).

The square resistance values (R^{\square}) obtained in this way are plotted in the inset of Fig. 1(c) as a function of V_G . They exhibit variations of at most 50 %, in large part due to the difficulty to define the device dimensions precisely when calculating R^{\square} , and to the geometry of the WS_2 flake, that results in a non perfectly uniform current distribution. Overall, therefore, these measurements indicate a reasonably good electrical homogeneity of the devices at room temperature, when the ionic gate is still in the liquid state.

To investigate low-temperature electronic transport upon accumulation of a high density of electrons, the device temperature was set just above the freezing point of DEME-TFSI,^{13,17,43} and the gate voltage applied. At this lower T possible chemical reactions between WS_2 and the ionic liquid slow down, enabling a much wider range of V_G to be applied without causing device degradation. Values of V_G between 3 and 6 V were applied in different measurement runs, after which the device was cooled down to the base temperature of our ^3He system (0.25 K). Throughout this procedure, the gate leakage current was monitored to ensure that it remained negligibly small (below 1 nA).

Figure 2(a) shows the temperature dependence of the square resistance at $V_G = 3.7$ V, obtained in a four-probe configuration by measuring the voltage between contacts 7 and 8 (see Fig. 1(a); a current bias of 30 nA was forced from S to D). Metallic transport is observed, with R^{\square} first decreasing as T is lowered to approximately 30-40 K, and then saturating to $R^{\square} \simeq 550\Omega$. Upon further cooling we see that, below approximately $T = 4$ K, the device exhibits a sharp, large decrease of resistance. Fig. 2(b) zooms-in on the behavior of $R^{\square}(T)$ below $T = 10$ K, making it apparent that at $T \simeq 4$ K, the device starts undergoing a transition to a zero resistance state, which is attained below $T = 0.4$ K. This is the first observation of a superconducting state in WS_2 . It demonstrates that the possibility of electrostatically inducing superconductivity in semiconducting TMDs is not confined to Mo-based compounds²⁷⁻²⁹ (the only ones in which the phenomenon had been reported so far).

To further substantiate that the zero-resistance state is a manifestation of superconductivity, we investigated transport in the presence of an applied perpendicular magnetic field. The mag-

netoresistance measured at $T = 0.25$ K is shown in the inset of Fig. 2(b). We find that a truly zero-resistance state persists only up to $B = 10$ G, and that at higher values of B the resistance increases rapidly, reaching the value measured in the normal state at $B = 0.14$ T (i.e., the critical field at $T = 0.25$ K is $B_C = 0.14$ T). For large field values the magnetoresistance is essentially negligible. Fig. 2(c) further shows the evolution of R^\square as a function of T , in the presence of different values of applied perpendicular field, which confirms how superconductivity is suppressed on a magnetic field scale of $B \approx 0.1$ T. The same data show that above 4 K virtually no change of resistance with magnetic field is observed, confirming that the critical temperature $T_C \approx 4$ K (rather surprisingly, T_C does not seem to shift significantly upon the application of a magnetic field; this may be related to the inhomogeneity present in the device, see below). To identify T_C more precisely, we subtract the resistances measured at $B = 0$ and 0.1 T (inset of Fig. 2(c)), from which we can see that the difference of the two resistances starts to deviate from zero for $T < 4.25$ K (i.e., $T_C = 4.25$ K).

We have also analyzed the current-voltage ($I - V$) characteristics, obtained by measuring voltage between contacts 7 and 8 as a function of I_{SD} . Fig. 2(d) and 2(e) show the evolution of the $I - V$ curves as a function of temperature (at $B = 0$ T; Fig. 2(d)) and of magnetic field (at $T = 0.25$ K; Fig. 2(e)). At $T = 0.25$ K with $B = 0$ T, the maximum supercurrent (i.e., the critical current) is $I_{SD} = 0.3 \mu\text{A}$. With increasing T or B the supercurrent is suppressed, and the $I - V$ curves become fully linear for $T > T_C$ or $B > B_C$, as expected. In Fig. 2(f), the evolution of critical current with magnetic field is shown more clearly in a two-dimensional (2D) color plot of the $I - |V|$ characteristics measured at base temperature as a function of B .

Having established the occurrence of an electrostatically induced superconducting state in ionic liquid gated WS_2 devices, we discuss some important aspects of its nature that could be determined from our experiments. A first, very important aspect regards the presence of a rather strong electronic inhomogeneity, which can be illustrated by several different measurements. For instance, Fig. 3(a) shows the low-temperature square resistance $R^\square(T)$ at $V_G = 3.7$ V obtained by using contacts S and D to current bias the device ($I_{SD} = 30$ nA), and different pairs of contacts (indicated according to the labeling of Fig. 1(a)) to measure the resulting voltage drop. In all measurements

the superconducting transition is clearly seen. However, the square resistance in the normal state, the value of critical temperature, and the resistance well below the superconducting transition all depend strongly on the contacts used to perform the measurements. The square resistance varies by almost one order of magnitude (in contrast with the rather homogeneous behavior observed at room temperature), T_C ranges between approximately 2 and 4 K (the range is even broader if we include data from all the device measured), and the remnant square resistance well below T_C varies between 0 to approximately 300 Ω . This type of behavior has been observed in all the different devices that we have measured, and upon cooling a same device multiple times. The inhomogeneity also manifests itself in large local variations of carrier density (approximately a factor of 4 across the entire device) extracted from Hall measurements performed with different pairs of contacts (see Fig. 3(b)). From all these observations we conclude that the electronic inhomogeneity needs to be taken into account in the interpretation of the experimental results. For instance establishing a well-defined relation between T_C and n is problematic, as shown in Fig. 3(c): if we plot all the data points available, any possible relation between T_C and n is eclipsed by the device inhomogeneity (establishing such a relation may be possible by selecting data according to some criterion, but it certainly remains important to check whether the result represents well the behavior of the experimental system).

In the superconducting state, the inhomogeneity also manifests itself in interesting ways that provide information about the underlying length scale. Fig. 3(d) shows the variation of $I - V$ curves upon finely varying the applied perpendicular magnetic field, on a scale of a few Gauss. An oscillatory behavior of the critical current is apparent, with a rather precisely well-defined period. These oscillations in critical current are a manifestation of quantum interference, the same mechanism responsible for the operation of SQUID devices.⁴⁴ Their observation implies the presence of a superconducting loop encircling a non-superconducting region, with the critical current responding periodically (with a period given by the superconducting flux quantum $h/2e$) to variations of the magnetic flux through the loop. From the period measured experimentally (0.36 Gauss) we estimate the area of the loop to correspond to a square of $7.6 \times 7.6 \mu\text{m}^2$ (compatible with the size of

the device area probed by the four-terminal measurements, which is approximately $25 \times 15 \mu\text{m}^2$). This observation –as well as all the measurements discussed above– are compatible with the inhomogeneity occurring over a rather large length scale (several microns; it appears possible that on a length scale of approximately 1 micron the homogeneity is significantly better). In the future it will be particularly important to determine the length scale associate to the inhomogeneous charge density in ionic liquid gated devices and find ways to substantially suppress this inhomogeneity.

We believe that the observed inhomogeneity originates from the frozen ionic liquid detaching locally from the surface of the WS_2 device (e.g., because of different thermal expansion coefficients), with the resulting increased distance between frozen liquid and the WS_2 surface causing a large decrease of geometrical capacitance, and correspondingly, of induced charge. Many observations support this idea. For instance, we found that measurements of all the four-terminal resistances in a device such as the one shown in Fig. 1(a) allow us to determine (at least approximately) the path followed by the current flowing from the S to the D contact, and provide clear evidence for large patches of the surface not being conducting. Another indication can be obtained by comparing the temperature dependence of the square resistance upon cooling and warming up the device (see Fig. 3(e)). Upon warming up the device, the resistance is significantly larger than that measured during cooling down (as a result of the detachment of the liquid), but as soon as the melting temperature of the liquid is reached (at approximately 200 K), the resistance recovers its original value. Indeed, as we discussed earlier on, when the ionic liquid is kept above its freezing point, the transport properties are rather homogeneous.

Another question worth investigating is whether the experiments provide evidence for the 2D character of the superconducting state, which can certainly be expected, since the thickness of the accumulation layer at carrier density values of $n \approx 10^{14} \text{ cm}^{-2}$ –determined by the electrostatic screening length– is only approximately 1 nm. To address this issue, we compare the behavior of the superconducting transition to theoretical expectations for 2D Berezinski-Kosterlitz-Thouless (BKT) superconductivity.^{35–41} One of the well-known properties of BKT superconductors is the occurrence of power law $I - V$ curves:^{40,41} $V \propto I^\alpha$ where $\alpha = 1$ for T well above T_{BKT} , $\alpha = 3$

for $T = T_{BKT}$, and $\alpha > 3$ for $T < T_{BKT}$ (T_{BKT} is the BKT transition temperature below which a finite stiffness of the phase of the superconducting parameter appears; it is smaller than the mean-field critical temperature⁴⁴ where superconductivity appears locally, without global phase coherence). Fig. 4(a) shows the $I - V$ curves measured well below the onset of superconductivity in log-log scale: the linear behavior observed (over one-to-two decades in current) reveals that a power law dependence does indeed hold. From the slope we extract the exponent α , whose T -dependence is shown in Fig. 4(b). $\alpha = 3$ at $T = 0.63$ K, providing a first estimate of T_{BKT} . More evidence for BKT behavior is revealed by the temperature dependence of the resistance close to T_{BKT} . Theoretically, it is expected that $R = R_0 \exp(-bt^{-1/2})$, with R_0 and b material dependent parameters, and $t = T/T_{BKT} - 1$.^{40,41} By plotting $[d(\ln R^{\square})/dT]^{-2/3}$ and extrapolating linearly this quantity to zero provides a second, independent way to determine T_{BKT} (see Fig. 4(c)). Following this procedure we obtain $T_{BKT} = 0.67$ K, in fairly good agreement with our previous estimate, indicating that at this level of analysis the experimental data are compatible with superconductivity having a 2D character.

Finally, we briefly compare electrostatically induced superconductivity on WS_2 to the same phenomenon observed on MoS_2 , as reported in Ref. 27. Overall, superconductivity in MoS_2 appears to be much more robust, with a significantly higher critical temperature (in excess of 10 K), surviving up to much larger magnetic field values (approximately 10 T at low temperature), showing critical currents orders of magnitude larger (Costanzo *et al.*, unpublished), and exhibiting a considerably narrower width of the superconducting transition as a function of temperature. Indeed, we have observed superconductivity in MoS_2 also in our laboratory, exhibiting features similar to those reported in Ref. 27. Similar to the findings discussed here, however, our measurements on MoS_2 also indicate the presence of inhomogeneity on a macroscopic scale, and a behavior compatible with 2D BKT superconductivity (our measurements on MoS_2 will be presented elsewhere).

In summary, we have investigated electronic properties of ionic liquid gated WS_2 exfoliated crystals and observed the first occurrence of superconductivity in this material. Next to char-

acterizing the superconducting properties, we have found that ionic liquid gated devices at low temperature exhibit a strong inhomogeneity that needs to be taken into account when analyzing the data, and observed that the measurements appears to be compatible with the behavior expected for 2D BKT superconductors.

Acknowledgement

We gratefully acknowledge T. Giamarchi and Y. Iwasa for discussions, and A. Ferreira for technical assistance. Financial support from the Swiss National Science Foundation, and from the EU Graphene Flagship is also gratefully acknowledged.

References

- (1) Wang, Q. H.; Kalantar-Zadeh, K.; Kis, A.; Coleman, J. N.; Strano, M. S. *Nature nanotechnology* **2012**, *7*, 699.
- (2) Chhowalla, M.; Shin, H. S.; Eda, G.; Li, L.-J.; Loh, K. P.; Zhang, H. *Nature chemistry* **2013**, *5*, 263.
- (3) Xiao, D.; Liu, G.-B.; Feng, W.; Xu, X.; Yao, W. *Phys. Rev. Lett.* **2012**, *108*, 196802.
- (4) Mak, K. F.; Lee, C.; Hone, J.; Shan, J.; Heinz, T. F. *Physical Review Letters* **2010**, *105*, 136805.
- (5) Splendiani, A.; Sun, L.; Zhang, Y.; Li, T.; Kim, J.; Chim, C.-Y.; Galli, G.; Wang, F. *Nano Letters* **2010**, *10*, 1271.
- (6) Cao, T.; Wang, G.; Han, W.; Ye, H.; Zhu, C.; Shi, J.; Niu, Q.; Tan, P.; Wang, E.; Liu, B.; Feng, J. *Nature communications* **2012**, *3*, 887.
- (7) Zeng, H.; Dai, J.; Yao, W.; Xiao, D.; Cui, X. *Nature nanotechnology* **2012**, *7*, 490.
- (8) Mak, K. F.; He, K.; Shan, J.; Heinz, T. F. *Nature nanotechnology* **2012**, *7*, 494.

- (9) Jones, A. M.; Yu, H.; Ghimire, N. J.; Wu, S.; Aivazian, G.; Ross, J. S.; Zhao, B.; Yan, J.; Mandrus, D. G.; Xiao, D.; Yao, W.; Xu, X. *Nature nanotechnology* **2013**, *8*, 634.
- (10) Mak, K. F.; McGill, K. L.; Park, J.; McEuen, P. L. *Science* **2014**, *344*, 1489.
- (11) Xu, X.; Yao, W.; Xiao, D.; Heinz, T. F. *Nature Physics* **2014**, *10*, 343.
- (12) Radisavljevic, B.; Radenovic, A.; Brivio, J.; Giacometti, V.; Kis, A. *Nature nanotechnology* **2011**, *6*, 147.
- (13) Zhang, Y.; Ye, J.; Matsushashi, Y.; Iwasa, Y. *Nano letters* **2012**, *12*, 1136.
- (14) Braga, D.; Gutiérrez Lezama, I.; Berger, H.; Morpurgo, A. F. *Nano letters* **2012**, *12*, 5218.
- (15) Radisavljevic, B.; Kis, A. *Nature materials* **2013**, *12*, 815.
- (16) Baugher, B. W. H.; Churchill, H. O. H.; Yang, Y.; Jarillo-Herrero, P. *Nano letters* **2013**, *13*, 4212.
- (17) Jo, S.; Ubrig, N.; Berger, H.; Kuzmenko, A. B.; Morpurgo, A. F. *Nano letters* **2014**, *14*, 2019.
- (18) Ovchinnikov, D.; Allain, A.; Huang, Y.-S.; Dumcenco, D.; Kis, A. *ACS nano* **2014**, *8*, 8174.
- (19) Gutiérrez Lezama, I.; Ubaldini, A.; Longobardi, M.; Giannini, E.; Renner, C.; Kuzmenko, A. B.; Morpurgo, A. F. *2D Materials* **2014**, *1*, 021002.
- (20) Sundaram, R. S.; Engel, M.; Lombardo, A.; Krupke, R.; Ferrari, A. C.; Avouris, P.; Steiner, M. *Nano Letters* **2013**, *13*, 1416.
- (21) Lopez-Sanchez, O.; Lembke, D.; Kayci, M.; Radenovic, A.; Kis, A. *Nature nanotechnology* **2013**, *8*, 497.
- (22) Pospischil, A.; Furchi, M. M.; Mueller, T. *Nature nanotechnology* **2014**, *9*, 257.
- (23) Baugher, B. W.; Churchill, H. O.; Yang, Y.; Jarillo-Herrero, P. *Nature nanotechnology* **2014**, *9*, 262.

- (24) Ross, J. S.; Klement, P.; Jones, A. M.; Ghimire, N. J.; Yan, J.; Mandrus, D. G.; Taniguchi, T.; Watanabe, K.; Kitamura, K.; Yao, W.; Cobden, D. H.; Xu, X. *Nature nanotechnology* **2014**, *9*, 268.
- (25) Ubrig, N.; Jo, S.; Berger, H.; Morpurgo, A. F.; Kuzmenko, A. B. *Applied Physics Letters* **2014**, *104*, 171112.
- (26) Zhang, Y.; Oka, T.; Suzuki, R.; Ye, J.; Iwasa, Y. *Science* **2014**, *344*, 725–728.
- (27) Ye, J. T.; Zhang, Y. J.; Akashi, R.; Bahramy, M. S.; Arita, R.; Iwasa, Y. *Science* **2012**, 338, 1193.
- (28) Taniguchi, K.; Matsumoto, A.; Shimotani, H.; Takagi, H. *Applied Physics Letters* **2012**, *101*, 042603.
- (29) Shi, W.; Ye, J. T.; Zhang, Y.; Suzuki, R.; Saito, Y.; Iwasa, Y. *APS March Meeting 2014* **2014**, <http://meetings.aps.org/Meeting/MAR14/Session/J52.2>.
- (30) Panzer, M. J.; Newman, C. R.; Frisbie, C. D. *Applied Physics Letters* **2005**, *86*, 103503.
- (31) Shimotani, H.; Asanuma, H.; Takeya, J.; Iwasa, Y. *Applied Physics Letters* **2006**, *89*, 203501.
- (32) Somoano, R.; Hadek, V.; Rembaum, A.; Samson, S.; Woollam, J. *The Journal of Chemical Physics* **1975**, *62*, 1068.
- (33) Woollam, J. A.; Somoano, R. B. *Materials Science and Engineering* **1977**, *31*, 289.
- (34) Yuan, H.; Bahramy, M. S.; Morimoto, K.; Wu, S.; Nomura, K.; Yang, B.-J.; Shimotani, H.; Suzuki, R.; Toh, M.; Kloc, C.; Xu, X.; Arita, R.; Nagaosa, N.; Iwasa, Y. *Nature Physics* **2013**, *9*, 563.
- (35) Berezinskii, V. L. *Soviet Physics JETP* **1972**, *34*, 610.
- (36) Kosterlitz, J. M.; Thouless, D. J. *Journal of Physics C: Solid State Physics* **1973**, *6*, 1181.

- (37) Kosterlitz, J. M. *Journal of Physics C: Solid State Physics* **1974**, 7, 1046.
- (38) Beasley, M. R.; Mooij, J. E.; Orlando, T. P. *Physical Review Letters* **1979**, 42, 1165.
- (39) Doniach, S.; Huberman, B. A. *Physical Review Letters* **1979**, 42, 1169.
- (40) Halperin, B. I.; Nelson, D. R. *Journal of Low Temperature Physics* **1979**, 36, 599.
- (41) Benfatto, L.; Castellani, C.; Giamarchi, T. *Physical Review B* **2009**, 80, 214506.
- (42) Horowitz, G.; Hajlaoui, M. E.; Hajlaoui, R. *Journal of Applied Physics* **2000**, 87, 4456.
- (43) Sato, T.; Masuda, G.; Takagi, K. *Electrochimica Acta* **2004**, 49, 3603.
- (44) Tinkam, M. *Introduction to Superconductivity*; Dover, 2004.

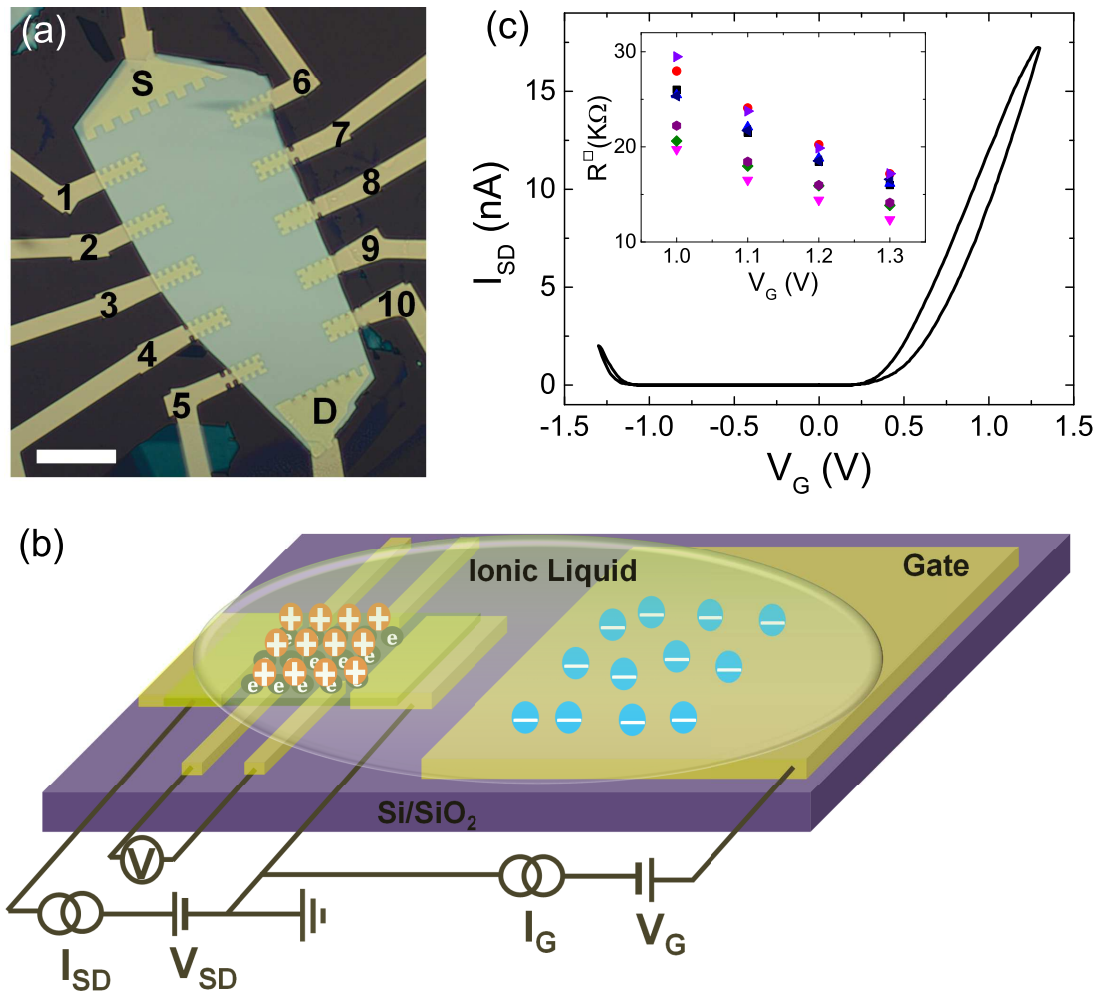


Figure 1: (a) Optical microscope image of a device used in our investigation (the WS_2 flake is 20 nm thick; the white bar is $15 \mu\text{m}$ long). The numbers (1 to 10) label the contacts used to probe the transport locally in the device, upon sending current from the source (S) to the drain (D) contact. The saw-tooth shape of the contacts is designed to increase the contact area, which helps to reduce the contact resistance. (b) Schematic illustration of our ionic liquid gated field effect transistors, under electron accumulation. (c) Source-drain current (I_{SD}) as a function of gate voltage (V_G) measured at room temperature with $V_{SD} = 1 \text{ mV}$. The inset shows the square resistance extracted from multi-terminal measurements performed using different contacts as voltage probe (1 and 2, 2 and 3, ..., 9 and 10).

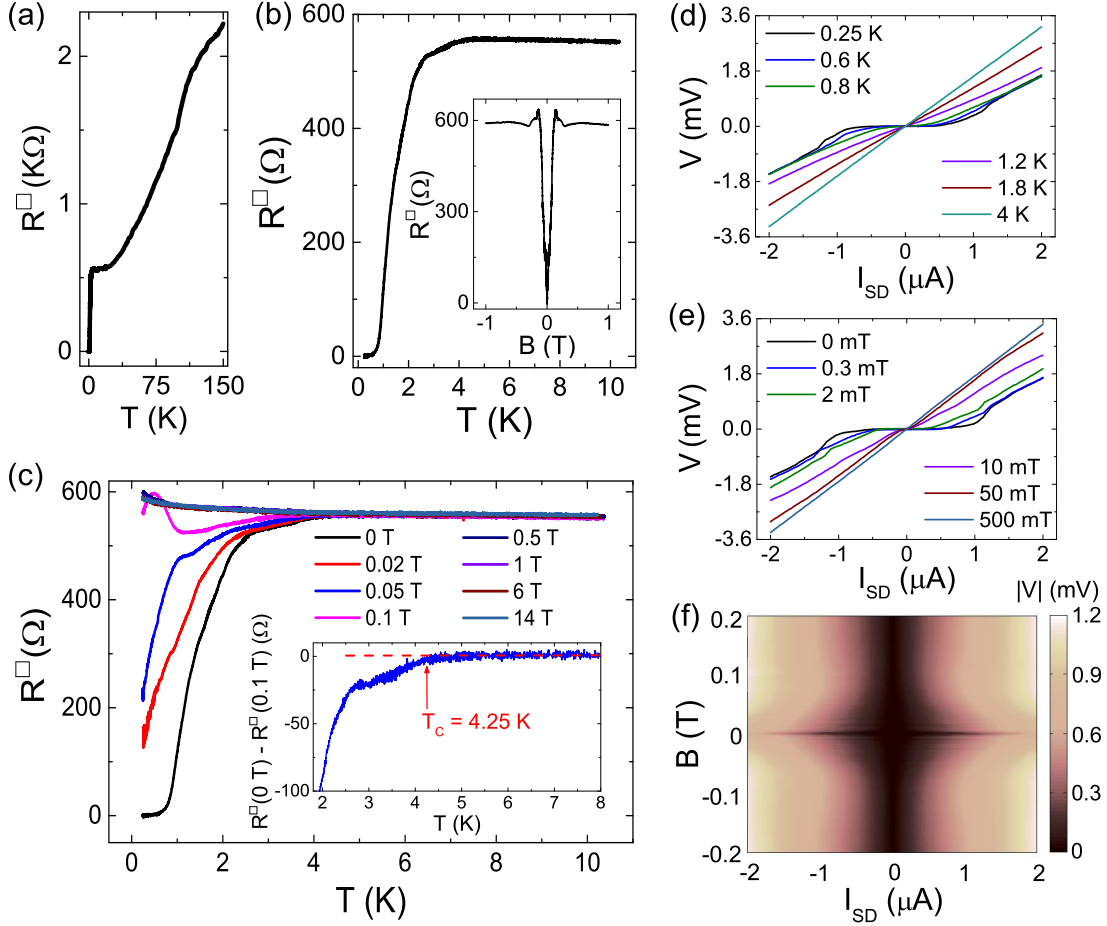


Figure 2: Four-probe transport properties recorded at $V_G = 3.7$ V by measuring the voltage between contacts 7 and 8, as a function of source-drain current I_{SD} . The observed temperature dependence of the square resistance reveals metallic behavior at higher temperatures (a), followed by a superconducting transition at lower T (b). The inset of panel (b) shows the magnetoresistance measured at $T = 0.25$ K. (c) Evolution of the T dependence of the square resistance, for different values of perpendicular magnetic field. The inset shows the quantity $R^\square(B = 0 \text{ T}) - R^\square(B = 0.1 \text{ T})$, which makes it possible to determine T_C more precisely. Evolution of current-voltage ($I - V$) characteristic as a function of T at $B = 0$ T (d) and as a function of B for $T = 0.25$ K (e). (f) Two-dimensional color plot of $I - |V|$ as a function of B .

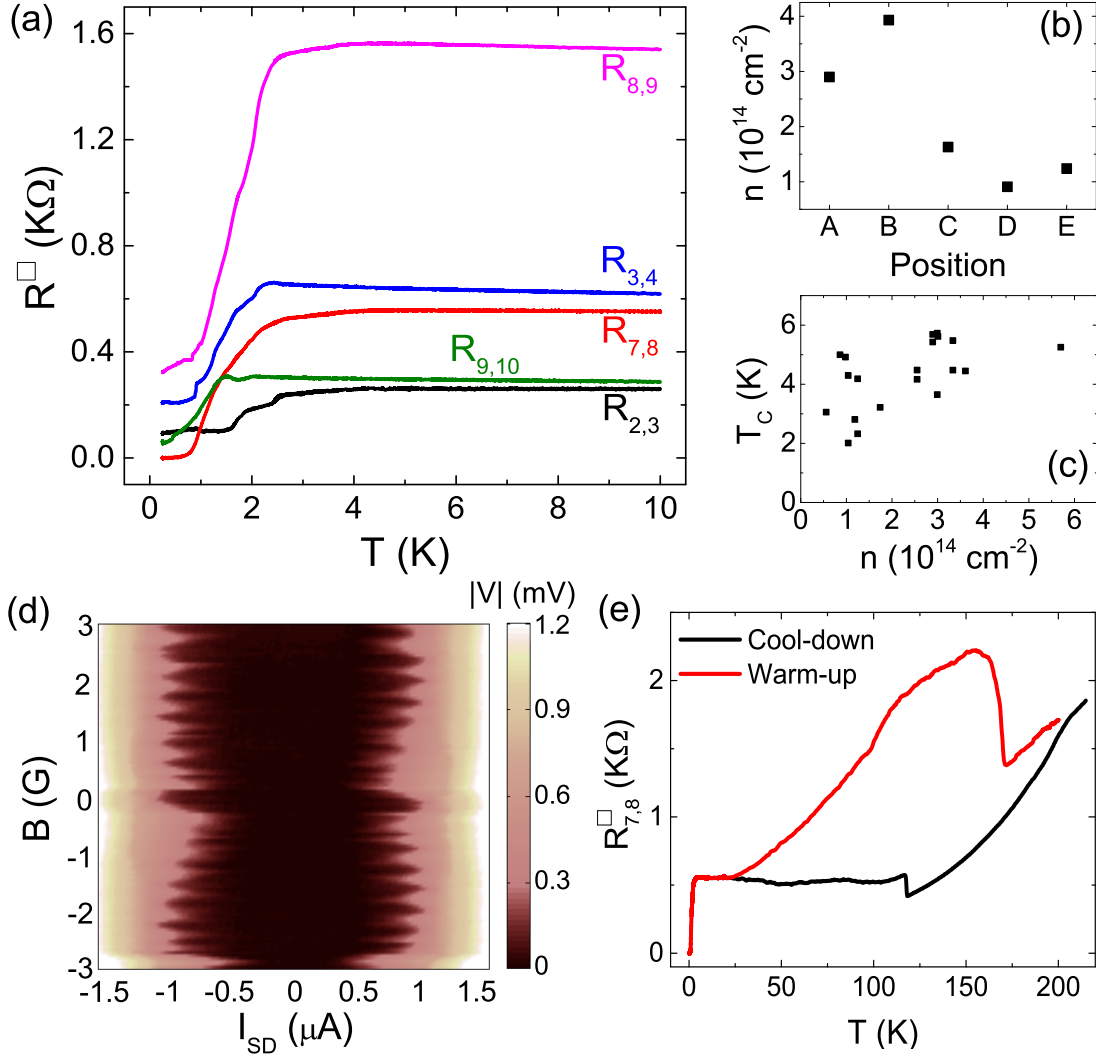


Figure 3: (a) Temperature dependence of the square resistance ($R^{\square}(T)$) measured in a four-terminal configuration, with different pairs of voltage probes ($V_G = 3.7$ V; $I_{SD} = 30$ nA), showing a considerable inhomogeneity. (b) Carrier density n extracted at $V_G = 3.7$ V from the measurement of the Hall effect at different positions in the device (each letter corresponds to measurements done with a different pair of contacts: A= contacts 1 and 6; B= 2 and 7; C= 3 and 8, D= 4 and 9, and E= 5 and 10, with the labeling of Fig. 1(a)). (c) T_C as a function of n , showing data obtained with different electrode pairs in the three different devices that we have studied. The large variations of n eclipses any systematic relation. (d) Color plot of the $I - |V|$ characteristic measured at low magnetic field B , showing a clear periodic oscillation of the critical current. (e) Square resistance $R^{\square}(T)$ measured as a function of T while cooling and warming up the device.

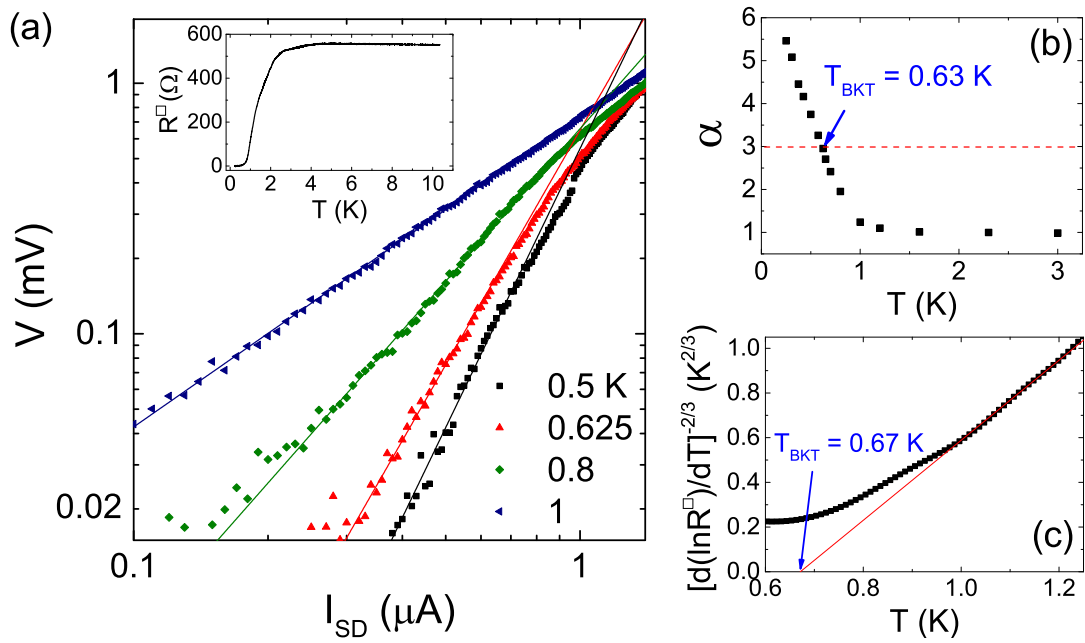


Figure 4: (a) Power law dependence $V \propto I^\alpha$ of the $I - V$ characteristics (V measured with the contacts of 7 and 8 as a function of I_{SD}) for different values of $T < T_C$. The solid lines are best fits done to extract the exponent α (the inset shows $R^\square(T)$ measured with the same contacts). (b) Temperature dependence of the exponent α . $T_{BKT} = 0.63$ K is determined by the condition $\alpha = 3$. (c) Plot of $[d(\ln R^\square)/dT]^{-2/3}$, with a linear extrapolation of the linear part, which provides an independent determination of T_{BKT} . This method gives $T_{BKT} = 0.67$ K, in fairly good agreement with the analysis of the $I - V$ curves.